RIJKSUNIVERSITEIT GRONINGEN

BACHELOR'S THESIS

Orbits and the velocity structure of stars near the Sun

Author:
Daniël KOOT

Supervisor:
Prof. dr. Amina HELMI
Dr. Lorenzo POSTI

A thesis submitted in fulfillment of the requirements for the degree of Bachelor of Sciencs

in the

Kapteyn Astronomical Institute

August 22, 2017

Rijksuniversiteit Groningen

Abstract

Faculty Name
Kapteyn Astronomical Institute

Bachelor of Sciencs

Orbits and the velocity structure of stars near the Sun

by Daniël KOOT

In this research project I have investigated the influence of a static long and a short bar on the structure in velocity space in the Solar neighbourhood compared to the results of an axisymmetric model. This has been done by integrating the orbits for 42773 stars within a range of $300pc$ of the Sun with a relative parallax error < 10%. After this, the positions and velocity distributions in the same area have been plotted to look at the differences in velocity space. It was found that the stars that originate from the Hercules stream do return in the same region in velocity space, but only after an even number of azimuthal periods in their own frame for the axisymmetric model. The short bar makes for shorter azimuthal periods than the long bar, which is similar to the axisymmetric model. The shape of the velocity distribution of the short bar is however more similar to the velocity distribution of the long bar. Since a static bar was used, there is no influence of bar resonance, which is believed to be the actual cause of the Hercules stream.

Contents

Abstract **i**

1 Introduction **1**

2 Theory **3**
2.1 Galactic Dynamics . . . 3
2.2 Potential Functions . . . 3
2.2.1 The Miyamoto-Nagai Potential . . . 3
2.2.2 The NFW Potential . . . 4
2.2.3 The Hernquist Potential . . . 4
2.2.4 Ferrers bar Potential . . . 4
2.3 Forces & Energy . . . 5
2.4 Leap Frog Integration . . . 6

3 Method **7**
3.1 Data and selection criterion . . . 7
3.2 Galaxy Potentials . . . 9

4 Results **13**
4.1 The Axisymmetric Potential . . . 13
4.2 The Triaxial Bar Potential . . . 18
4.2.1 The Long bar . . . 18
4.2.2 The Short bar . . . 18

5 Conclusion & Discussion **24**

Acknowledgements **25**

A Code **26**
A.1 Program Explanation . . . 26
A.2 Leap Frog . . . 27
A.3 Ferrers Potential . . . 29
A.4 Ferrers addition I . . . 30
A.5 Ferrers addition II . . . 31

Chapter 1

Introduction

A galaxy is a system in space that consists of several mass components, namely stars, gas and dark matter. All these components have an influence on the system as a whole but the mutual gravitational attraction that they experience is what holds them together in a galaxy like the Milky Way. The Milky Way is a spiral galaxy, which can be considered as the superposition of the components described below (see figure 1.1).

The disk-component is the most well-known part of the galaxy and commonly the most recognizable part. This is mostly due to its spiral arms, which have a very characteristic view. The halo-component however is much less understood. The leading theory is that we speak of a Dark-Matter halo. This can be explained as a halo made by matter of unknown nature that accounts for the missing mass typically needed to explain the observed rotation curves of spiral galaxies.

The central component of a galaxy can have a large variety of shapes. In some galaxies we detect just a smooth transition from the disk to the center, in some galaxies we detect a bulge and in other galaxies we detect a bar. The latter has been brought into attention for our own Galaxy, since scientists have discovered that the Milky Way is barred galaxy after observations of gas velocities and infrared photometry (De Vaucouleurs, 1964; Peters III, 1975; Cohen and Few, 1976; Liszt and Burton, 1980; Blitz and Spergel, 1991; Binney, Gerhard, and Spergel, 1997; Raboud et al., 1998).

In this research project I will consider the influence of either a long or a short bar on large scale structures in velocity space in the Solar neighbourhood (SNd). The structure I will focus on is the Hercules stream. The Hercules stream is a substantial group of stars trailing behind the Galactic rotation and having a positive outwards velocity (Raboud et al., 1998; Dehnen, 2000; Bissantz and Gerhard, 2002; Famaey et al., 2005; Bensby et al., 2007; Famaey, Siebert, and Jorissen, 2008; Monari et al., 2017). We can describe this as an overdensity of stars within the vicinity of the Sun. Their velocity is in the order of $40 - 50 km/s$ slower than the Local Standard of Rest (LSR). The LSR is a hypothetical star at the distance of the Sun from the Galactic center with a tangential velocity that matches the circular velocity in the rotation curve at that distance.

My aim is to look at how this structure evolves in time. I will be doing this by using data from Gaia and RAVE. Gaia is a satellite that has been launched to map the positions and velocities of over a billion stars to be able to make an accurate 6D map of the Milky Way (ESA, 2005). RAVE (RAdial Velocity Experiment) was set up to measure the line-of-sight velocities of nearby stars to study their motions in the thick and thin disk and the stellar halo of the Milky Way (RAVE, 2014). Using these datasets combined can help in investigating the formation and structure of the Galaxy.

Altogether, I am now able to formulate a research question which I will try to answer at the end of the thesis. The question is: What is the influence of a long and a short bar on large scale velocity structures and are these structures long-lived?

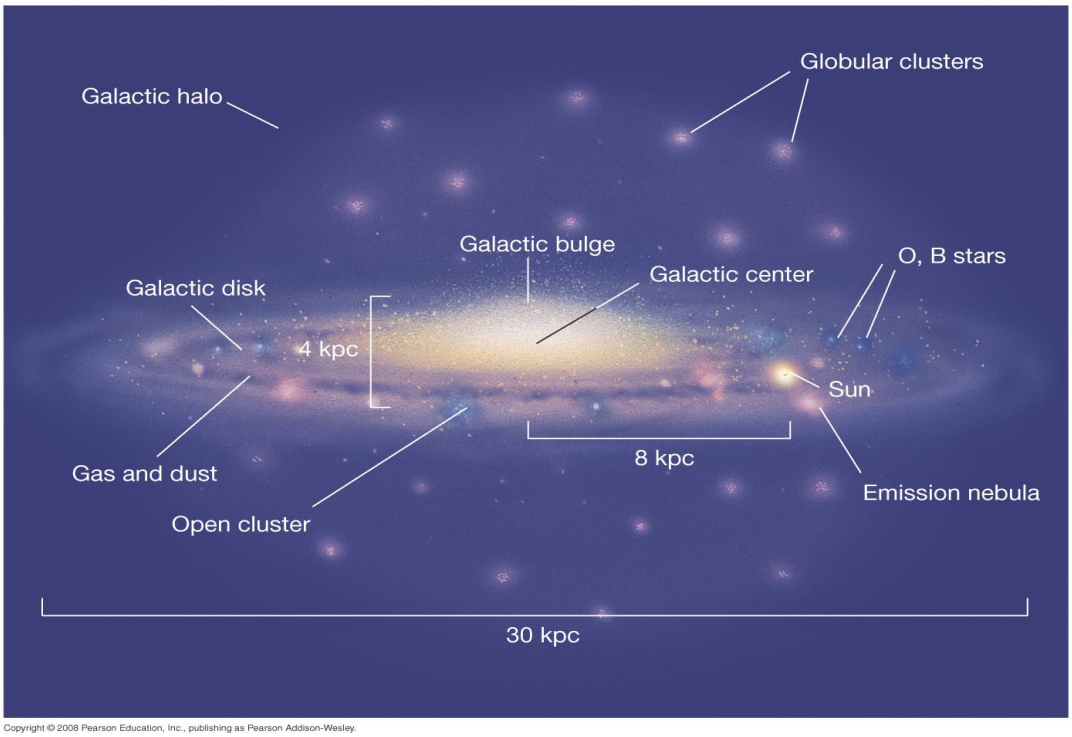

Figure 1.1: The structure of the Milky Way

©Pearson, 2008

In chapter 2 I will explain the underlying theory for galactic potentials and orbital mechanics. In chapter 3 I will describe the method I used. This will include a section about the data and the design of the Galactic models. In Chapter 4 the results are described. Finally, chapter 5 contains an overall conclusion and discussion of the results and the entire research project.

Chapter 2

Theory

The main goal of this chapter is to give an explanation of the theory used in this research project. This contains the intrinsic forms and explanations of different potential functions, but also how to apply them and their relation to orbital mechanics. Furthermore, I will do an introduction on the Leap Frog algorithm to solve numerically the equations of motion.

2.1 Galactic Dynamics

The basis of this thesis is the kinematics that make stars in a galaxy behave the way they do. This involves their bulk movement as well as their random motions. By measuring these motions one can create a model for the galaxy. As described earlier, the Galaxy can be described by 3 components. Hence any realistic model must have such 3 components. Each of these components has got a model on its own, which superposed make up for the entire galaxy model. The crux of the models lies in a density profile which can be converted to a potential function. Their relation is given by the Poisson equation:

$$\nabla^2\Phi = 4\pi G\rho, \tag{2.1}$$

where Φ is the potential, G is the gravitational constant and ρ is the mass density function.

2.2 Potential Functions

In this section the different potential functions, which are relevant for the Galactic model, will be treated. These include the Miyamoto-Nagai, the Navarro-Frenk-White (NFW), the Hernquist and the Ferrers Bar Potentials. Their forms as well as their roles in the full galactic model will be explained.

2.2.1 The Miyamoto-Nagai Potential

In 1975, Miyamoto and Nagai generalized the potentials, constructed by Kuzmin (1956) and Plummer (1911), as follows

$$\Phi(R,z) = \frac{GM_d}{\sqrt{R^2 + (a + \sqrt{z^2 + b^2})^2}}, \tag{2.2}$$

where M_d the mass of the disk, R the radius from the center in the plane, a is the scale length, b is the scale height and z is the distance above the plane. a and b both are non-zero constants with dimension of length (Miyamoto and Nagai, 1975).

The Miyamoto-Nagai Potential is commonly used as a model for the galactic disk. By varying the parameters a and b, the ratio $\frac{b}{a}$ will change, resulting in different shapes for the model. A very low ratio of $\frac{b}{a}$ will result in an almost flat disk, while a high ratio of $\frac{b}{a}$ will go towards a spherical system (Miyamoto and Nagai, 1975).

2.2.2 The NFW Potential

The second component of the galactic model is the NFW Potential. This potential, set up by Navarro, Frenk & White (Navarro, 1996), is very commonly used as a model for Dark Matter Halos. It is defined as follows

$$\Phi(r) = -\frac{4\pi G\rho_0 R_s^3}{r}\ln(1+\frac{R_s}{r}), \tag{2.3}$$

where R_s is the scale radius and ρ_0 is a characteristic value for the density, defined as

$$\rho_0 = \frac{M_H}{4\pi R_s^3}(\ln(1+c) - \frac{c}{1+c}), \tag{2.4}$$

where M_H is the mass of the halo and c is the concentration, which is defined as

$$c = \frac{R_{vir}}{R_s}, \tag{2.5}$$

where R_{vir} is the virial radius, which is a measure of the extent of the halo (Navarro, 1996).

2.2.3 The Hernquist Potential

The last part of the galactic model describes the central region of the galaxy, also referred to as the bulge. This potential is defined as follows

$$\Phi_b(R,z) = -\frac{GM_b}{r+R_c}, \tag{2.6}$$

where M_b is the mass of the bulge and R_c is the scale parameter (Hernquist, 1990).

When looking at the equation, the comparison with the regular Kepler Potential can be made very straightforwardly. The difference between a Hernquist Potential and a Kepler Potential is the constant R_c in the denominator of the Hernquist Potential. This can be described as the radius where the potential tends to a constant. Since the central region of the Milky Way is known to have a bar (De Vaucouleurs, 1964; Raboud et al., 1998; Bissantz and Gerhard, 2002), the replacement of this part of the potential is essential for this research project.

2.2.4 Ferrers bar Potential

In this research project the goal is to find the influence of the Milky Way bar on the stars in the Hercules stream, hence I need to replace the axisymmetric Hernquist bulge with a bar component and then compare the results in both cases.

The potential I will use to represent the bar is a Ferrers Potential. The structure of this potential can be seen in the following equation.

$$\Phi(x,y,z) = -\pi G a b c \frac{\rho_c}{n+1} \int_\lambda^\infty \frac{du}{\Delta(u)} (1 - m^2(u))^{n+1}, \tag{2.7}$$

where n is the logarithmic slope of the Ferrers density,

$$\rho_c = \frac{105}{32\pi} \frac{Mb}{abc}, \tag{2.8}$$

$$m^2 = \frac{x^2}{a^2+u} + \frac{y^2}{b^2+u} + \frac{z^2}{c^2+u}, \tag{2.9}$$

where *a*, *b* and *c* are the semi axes of the ellipsoid and λ is the unique positive solution of

$$m^2(\lambda) = 1, \tag{2.10}$$

When expanding the integral, coefficients can be calculated using recurrence relations to reduce integration time. See Pfenniger (1984) for the entire expansion of the potential and the definition of the forces using these coefficients for a logarithmic slope of the Ferrers density $n = 2$. Looking at the function m^2, it is very well visible that we are indeed dealing with an ellipsoidal object. Especially for $\lambda = 0$, the expression reduces to the equation of an ellipsoid. When the object that is integrated is within the boundaries of the bar (e.g. m<1), lambda is set to 0, which changes the boundaries of the integral.

2.3 Forces & Energy

The most important part of this research project is solving the equations of motion, in order to get the orbit of stars in a given potential. The equation of motion is

$$\ddot{x} = \vec{F}, \tag{2.11}$$

where $\ddot{x}$ is the second derivative of the position, also known as the acceleration and where $\vec{F}$ is the force per unit mass that is acting on the object. The force can also be defined as

$$\vec{F} = -\vec{\nabla}\Phi, \tag{2.12}$$

where $\vec{\nabla}\phi$ is the gradient of the potential (Landau, 1969).

In a stationary system the total energy of a system per unit mass

$$E = \frac{V_R^2 + V_\phi^2 + V_z^2}{2} + \Phi, \tag{2.13}$$

is conserved. In the integration of the equation of motion I will verify that the energy is indeed conserved by the algorithm and I will use this property as a quality criterion for the integrations.

2.4 Leap Frog Integration

The core part of this research project is the integration of the orbits for the provided stars. The most efficient way to do so is by means of a Leap Frog integrator.

A Leap Frog is a symplectic integrator. This comes with the consequence that it intrinsically conserves energy and that it is in fact time-reversible. The algorithm itself can be explained as follows: Contrary to the commonly used simultaneous updating of the position and velocity, they are being updated while being out of phase. In other words, in order to update one, you need the other at half the time-step, so that they leap over each other; hence the name. The equations of motion that will be solved at each time step are described below:

$$x_{i+1} = x_i + \delta t v_{i+\frac{1}{2}}, \tag{2.14}$$

$$v_{i+\frac{3}{2}} = v_{i+\frac{1}{2}} + \delta t \Phi_{x_i}, \tag{2.15}$$

where δt is the time step of the integration, Φ_{x_i} is the potential at position i and

$$v_{\frac{1}{2}} = v_0 + \frac{\delta t}{2} \Phi_{x_0}. \tag{2.16}$$

For a more schematic view of the Leap Frog, see the image below.

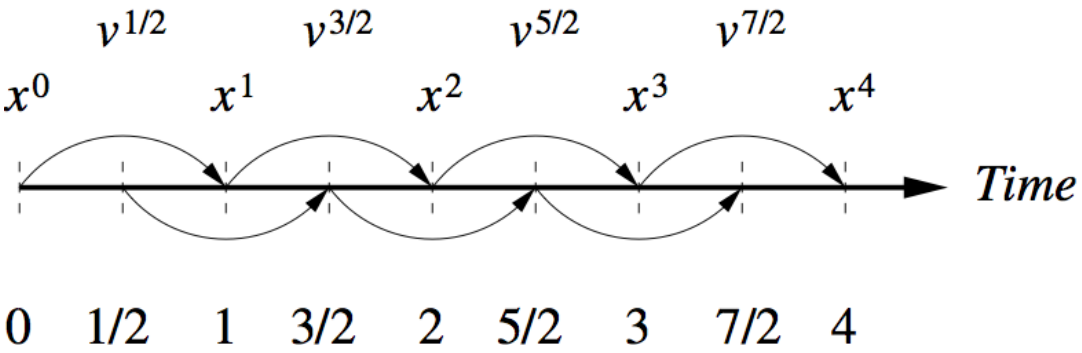

Figure 2.1: A visual representation of the Leap Frog method
©Krumholtz, 2015

It is clearly visible that the position and velocity take turn in being updated.

Chapter 3

Method

In this chapter, I will explain the way in which I obtained the results. First I will discuss how the data is selected. Then I will treat the different galactic models.

3.1 Data and selection criterion

The data that I will be using in this research project comes from TGAS and the RAVE. TGAS, short for Tycho-Gaia astrometric solution, is a joint solution of the positions from the Tycho-2 Catalogue with early Gaia data (Michalik, Lindegren, and Hobbs, 2015). RAVE is a spectroscopic survey, which has measured over half a million spectra and radial velocities (RAVE, 2014). The databases of TGAS and RAVE have a lot of sources in common and therefore they have been cross-matched to get the sample of stars that I will be using.

The vast majority of the stars are located within a few kpc from the Sun, where many interesting kinematic substructures are known to exist (Eggen, 1958). One of these structures is the Hercules stream. This is a group of stars trailing behind the galactic rotation and having a positive radial velocity (Raboud et al., 1998; Famaey et al., 2005; Bensby et al., 2007; Becker and Contopoulos, 2012; Famaey, Siebert, and Jorissen, 2008). A possible explanation for the existence of the Hercules stream is that it is caused through one of the resonances of by the Galactic bar (Dehnen, 2000; Antoja et al., 2014; Bovy, 2010; Monari et al., 2017; Pérez-Villegas et al., 2017). Both Outer Lindblad Resonance (OLR) and Corotation of the bar have been used in the analysis of the Hercules stream.

An important characteristic for the Hercules stream is its tangential velocity. Since the stars lag behind the galactic rotation, they have a lower velocity than the stars orbiting on circular orbits. Their velocity compared to the V_{LSR} is approximately $50km/s$ slower. This can be seen in Figure 3.1.

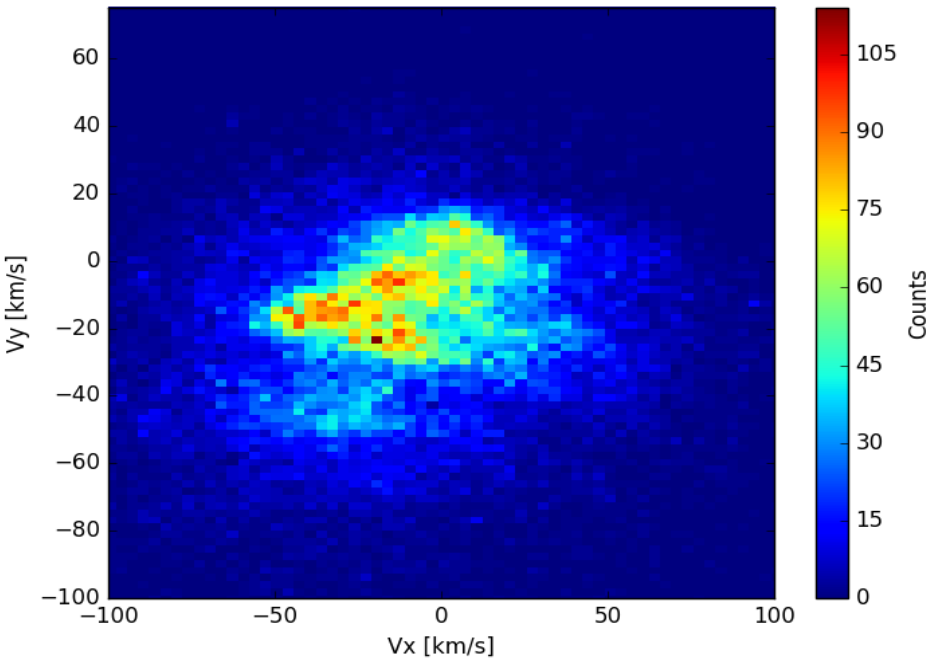

Figure 3.1: A plot of the cross-matched data of TGAS and RAVE containing 42773 stars within a range of $300pc$ with a relative parallax error < 10%.

In Figure 3.1 I plot the local velocity field on the disc of the galaxy for ≈ 40.000 stars within a distance of $300pc$ of the Sun. The quality criterion for this sample is a relative parallax error < 10%.

When analyzing the Vx-Vy plot for all the stars in the sample, it is very well noticeable that there is a concentration of stars with velocities in the range between $-50km/s$ < Vx < $-10km/s$ and $-60km/s$ < Vy < $-40km/s$. This is the region of interest, since here are the stars that belong to the Hercules stream. Other peaks in this plot are due to other local over-densities (e.g. the Pleiades in the range between $-20km/s$ < Vx < $-40km/s$ and $-10km/s$ < Vy < $-25km/s$ (Famaey, Siebert, and Jorissen, 2008)).

Figure 3.1 is in Heliocentric coordinates. This means that the plot is centered on the Local Standard of Rest. The LSR is a hypothetical star at $R_\odot = 8.3kpc$ and $V_{LSR} = (0, 228, 0)km/s$, which should move on a circular orbit in the Galactic potential. The peculiar velocity is defined at $V_{peculiar} \simeq (11, 12, 7)km/s$. This is the motion of the Sun with respect to the LSR, which can also be explained as the deviation from a purely circular orbit (Schönrich, 2012). The data itself, however, was handed to me in Galactocentric Cylindrical coordinates. So first of all I transformed the data from Cylindrical to Cartesian coordinates using the following formulae.

$$x = R\cos\phi, \tag{3.1}$$

$$y = R\sin\phi, \tag{3.2}$$

where R is the distance to the galactic center and ϕ is the angle with respect to the center of the galaxy. The velocities are transformed as follows:

$$V_x = V_R\cos\phi - V_\phi\sin\phi, \tag{3.3}$$

$$V_y = V_R \sin\phi + V_\phi \cos\phi, \tag{3.4}$$

where V_R and V_ϕ are the radial and tangential velocity respectively. This I could then use to integrate the orbits using my Cartesian Leap Frog.

3.2 Galaxy Potentials

In order to make the integrations for the stars, I first need to fully specify the Galactic Potentials. The Galaxy components I will use are parametrized in tables 3.1 and 3.2.

It is visible in table 3.1 that for the Miyamoto-Nagai potential the ratio $\frac{b}{a} \ll 1$. This means we are dealing with a flat disk. For the Ferrers potentials, it is visible in table 3.2 that the masses are equal and only the semi axes of the bar differ. However, the ratios of the axis stay constant so that the short bar is only a scaled down version of the long bar. Both the short and the long bar are oriented at an angle of $\phi = -28°$ with respect to the galactic center.

In order to use these potentials, I have written a program which can integrate the orbits for the stars in the sample. This comes with the implementation of the potentials themselves. But where the Disk, Halo and Axisymmetric Bulge have a clear formula for the potential, the Ferrers Bar Potential has got some complications. Namely, there is not an obvious formula that describes this potential. Therefore I decided to use a paper by Pfenniger (1984), who devised a formalism to write down the potential and the forces in Cartesian coordinates. The expressions for the potential and the forces contain 19 different coefficients which either can be calculated by numerical integration or by using the recurrence relations he has given in that paper. These recurrence relations will reduce the amount of integrations from 19 to 2. This has an enormous impact on the computational time.

These potentials can be implemented resulting in the contour plots of Figure 3.2. For each of the cases both the X vs Y and the X vs Z projection are visible. The axisymmetric potential has got a symmetric contour plot, where it is visible that the lines gradually separate more as a function of radius. Here the characteristic power-law shape of the Hernquist Potential is very clear. Now looking at the long bar compared to the short bar it is visible that the short bar has got a much more negative value for the potential, which is due to the fact that the mass is concentrated more in the center.

Table 3.1: Parameters for the potentials.

Potential	$Mass(M_\odot)$	a*	b*	R_s*	R_{vir}*	R_c*
Miyamoto-Nagai	$9.3 * 10^{10}$	6.5	0.26	-	-	-
NFW	$1.3 * 10^{12}$ (Axisymmetric) $0.8 * 10^{12}$ (Long Bar) $0.85 * 10^{12}$ (Short Bar)	-	-	15.3	245	-
Hernquist	$3.1 * 10^{10}$	-	-	-	-	0.7

* all in kpc

Table 3.2: Parameters for the bar potentials

Potential	$Mass(M_\odot)$	Fa*	Fb*	Fc*	n
Long Bar	$1.88 * 10^{10}$	5.0	2.12	1.59	2
Short Bar	$1.88 * 10^{10}$	3.5	1.4	1.1	2

* all in kpc

The rotation curves have been constructed in the following way. The circular velocity V_c is the tangential velocity of a star moving on a circular orbit at a distance R and is given by:

$$V_c^2(R) = R \left| \frac{\partial \Phi}{\partial R} \right|, \tag{3.5}$$

where $\frac{\partial \Phi}{\partial R}$ is the derivative of the potential with respect to R (Binney and Tremaine, 2011). For each component of the model a curve can be calculated and these can be superposed to make a complete image of the rotation curve of the model.

For all the models I set the circular velocity $V_{circ} = 228km/s$ at $R_\odot = 8.3kpc$. In order to have models with comparable contributions from the disc and bulge/bar, their masses are set in advance, hence the only variable component to adjust the rotation curve such that $V_{circ} = 228km/s$ at $R_\odot = 8.3kpc$ is the Dark Matter Halo. That is the reason why the NFW mass is not equal in the models. In the case of the barred potentials, I have plotted the circular velocity along the x-axis.

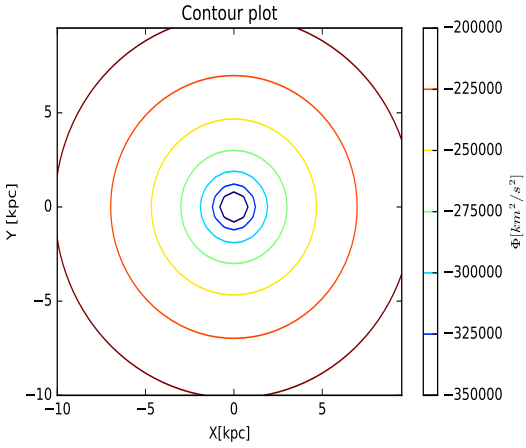

(a) Contour Axisymmetric model

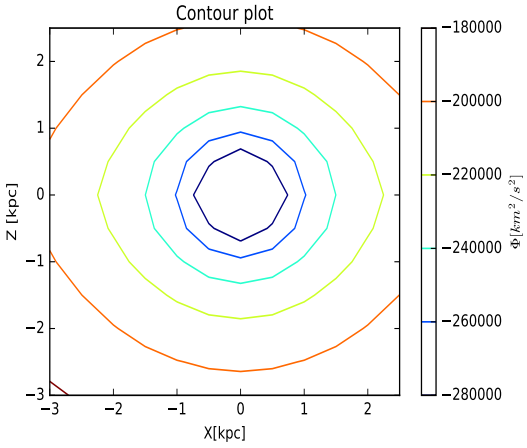

(b) X vs Z Contour

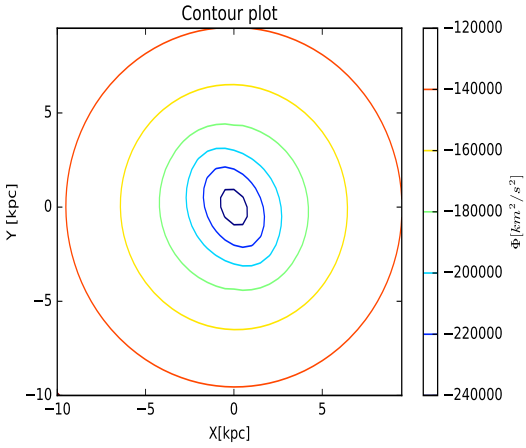

(c) Contour Long Bar model

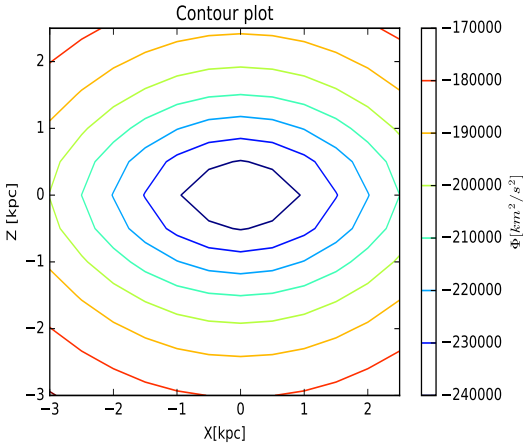

(d) X vs Z Contour

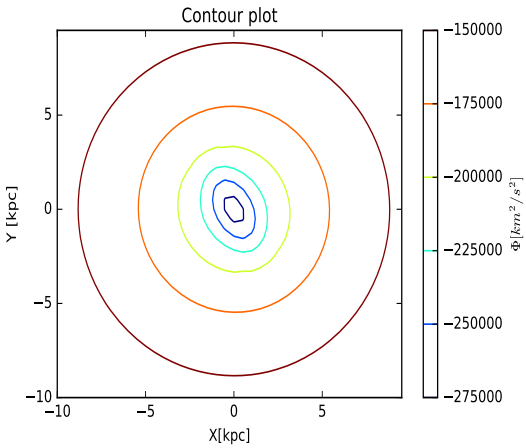

(e) Contour Short Bar model

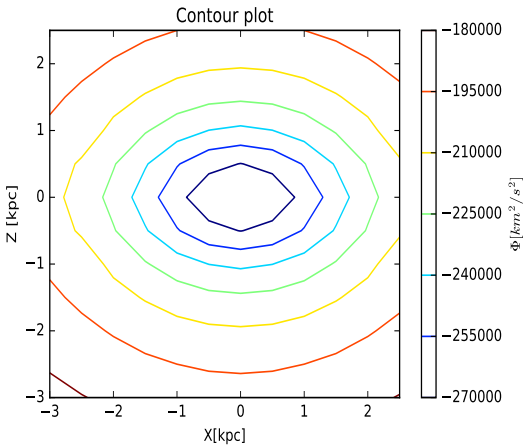

(f) X vs Z Contour

Figure 3.2: Contour plots of the potentials of the different Galactic models. Every model also contains a disk and a halo component.

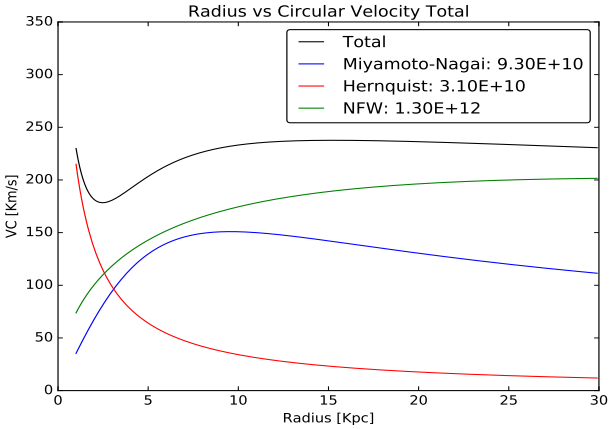

Figure 3.3: Rotation curve of the Axisymmetric Model along the x-direction

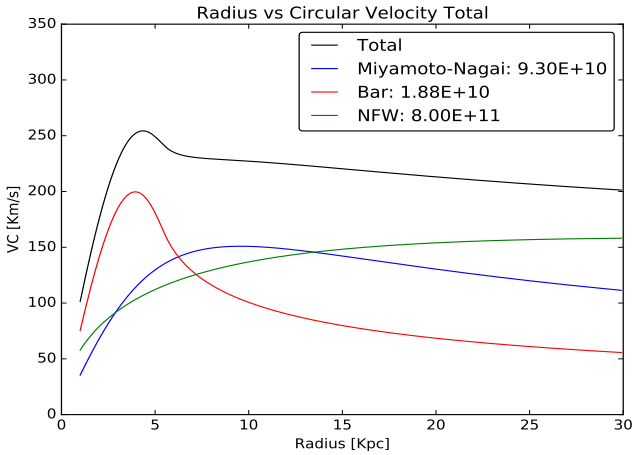

Figure 3.4: Rotation curve of the Long Barred Model along the x-direction

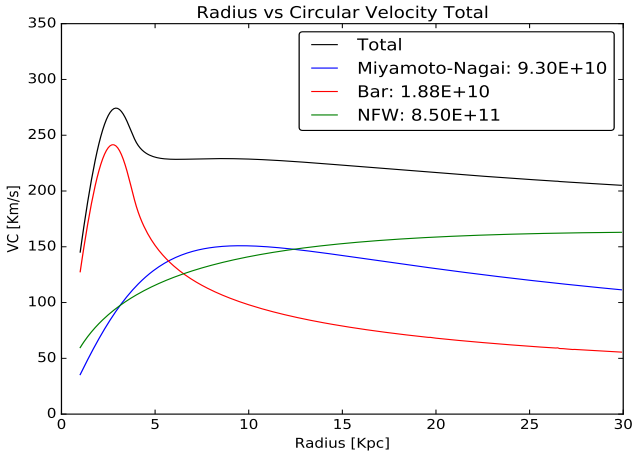

Figure 3.5: Rotation curve of the Short Barred Model along the x-direction

Chapter 4

Results

The Hercules stream is a known overdensity in velocity space. The question is whether or not the stars come back after a certain amount of time, such that we can or cannot speak of a long-lived structure. I want to consider 3 different cases: The axisymmetric case and the triaxial barred potential cases for a short and a long bar. In the axisymmetric case the Hernquist Potential is used for the bulge, while in the non-axisymmetric case we consider the Ferrers Bar Potential. In all the cases also a halo and a disk component are used. This chapter will treat the results I got by the orbit integration. As was described earlier, the stars should conserve energy. In practice, because of the precision of the integration, this is strictly not true. However, it is possible to modify the integration time step to obtain a certain threshold of energy conservation. I will consider only stars for which the energy is conserved to 5 %.

A consequence of this margin is that for the axisymmetric potential 99.9 % of the stars can be used for the analysis. For the barred potentials it means that 98.2 % of the stars conserve energy within a 5 % margin.

4.1 The Axisymmetric Potential

For the axisymmetric case I integrated the orbits with a Hernquist potential as the central potential for a time of 0.5 Gigayears, which is just over two azimuthal periods for the LSR. An azimuthal period is defined as the time it takes for a star to reach its initial azimuth:

$$\phi(t0 + t) = \phi(t0) \tag{4.1}$$

where ϕ is the azimuth of the star.

The orbits themselves have the shape shown in Figure 4.1.

As I expect for an axisymmetric potential, the trajectory is close to circular for a star that resembles the conditions of the LSR and it seems to come back at the same point after 1 azimuthal period. Also the position in the x-direction with respect to the z-direction gives a nice oscillatory motion as expected. The trajectory for the star originating from the Hercules stream is much less close to circular. It could be described as a rosette shaped trajectory.

At this point it is useful to take a look at the velocity distribution of all the stars in the sample and see how it changes over time. Figure 4.2 displays the initial velocity and position distribution of all the stars in the sample. The white box marks the region in velocity space, which is known as the Hercules stream and I plotted all stars in this box with red dots.

In Figure 4.3 one can see several frames of the position distributions for all the stars at different times. The top frames show the distribution after 1 azimuthal period with respect to the LSR. The middle frames are at 330 and 340 Myr, which coincides with twice the azimuthal period of the Hercules stream. The bottom frames show the distribution at 360 and 370 Myr, thus slightly later, and this is roughly twice the azimuthal period of the LSR.

The first thing that stands out is that nearly all of the Hercules stars seem to have a lead on the rest of the stars. Figure 4.4 shows the velocity distribution at the same times of the stars that are within the Solar neighbourhood. After the first azimuthal period of the LSR it is visible that the Hercules stars do not return in the Solar neighbourhood and that there is a rather smooth velocity distribution. There does not really seem to be any structure in the velocity distribution.

This lack of stars from Hercules after 1 azimuthal period can be explained by looking at the trajectories of the stars. From Figure 4.1 it is clear that a star in Hercules does not return in the Solar neighbourhood after 1 azimuthal period. On the contrary a star that resembles the LSR does return in the same region after each azimuthal period. This is due to the angular momentum of the star. Namely, in an axisymmetric potential the z-angular momentum should be conserved. For a star on a circular orbit, the angular momentum it has is the largest given its energy. However, when a star does not have the velocity of the LSR at $\sim R_{\odot}$, it will follow a different trajectory that also oscillates in the radial direction. In the case of a Hercules star this

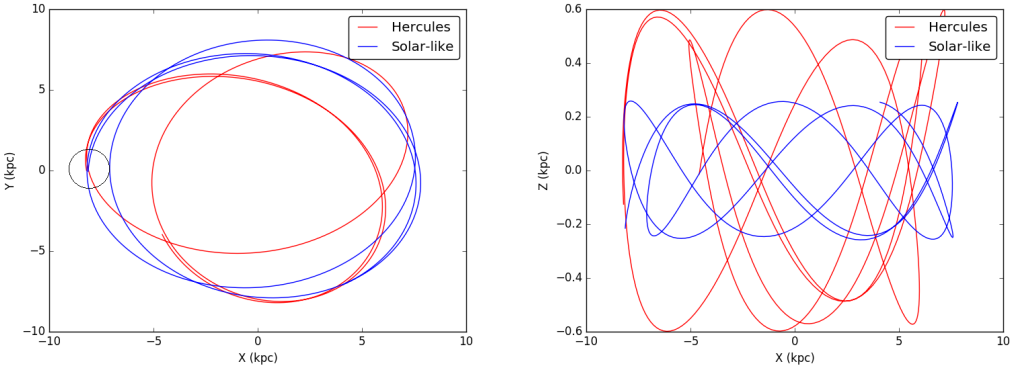

(a) Trajectory in X-Y plane (The circle resembles the SNd)

(b) Trajectory in X-Z plane

Figure 4.1: Trajectories in an axisymmetric potential.

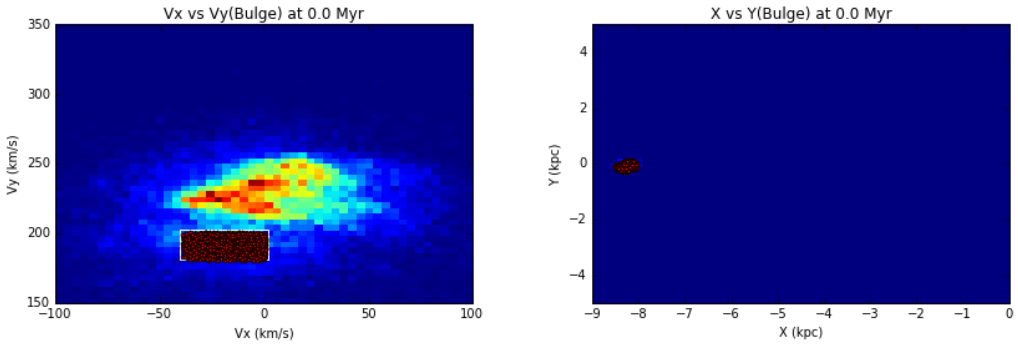

(a) Initial Velocity Distribution

(b) Initial Position Distribution

Figure 4.2: Initial conditions for the velocity and position distribution

means that after the first azimuthal period it does not have enough angular momentum to return to the same location, whereas other stars in the sample closer to the LSR can get back at their initial position.

After $330Myr$ the stars in Hercules return in the Solar neighbourhood and with that also in the white box, which specifies their initial conditions.

Lastly, after 2 azimuthal periods of the LSR it is visible that there is a smooth velocity distribution and there does not seem to be any structure.

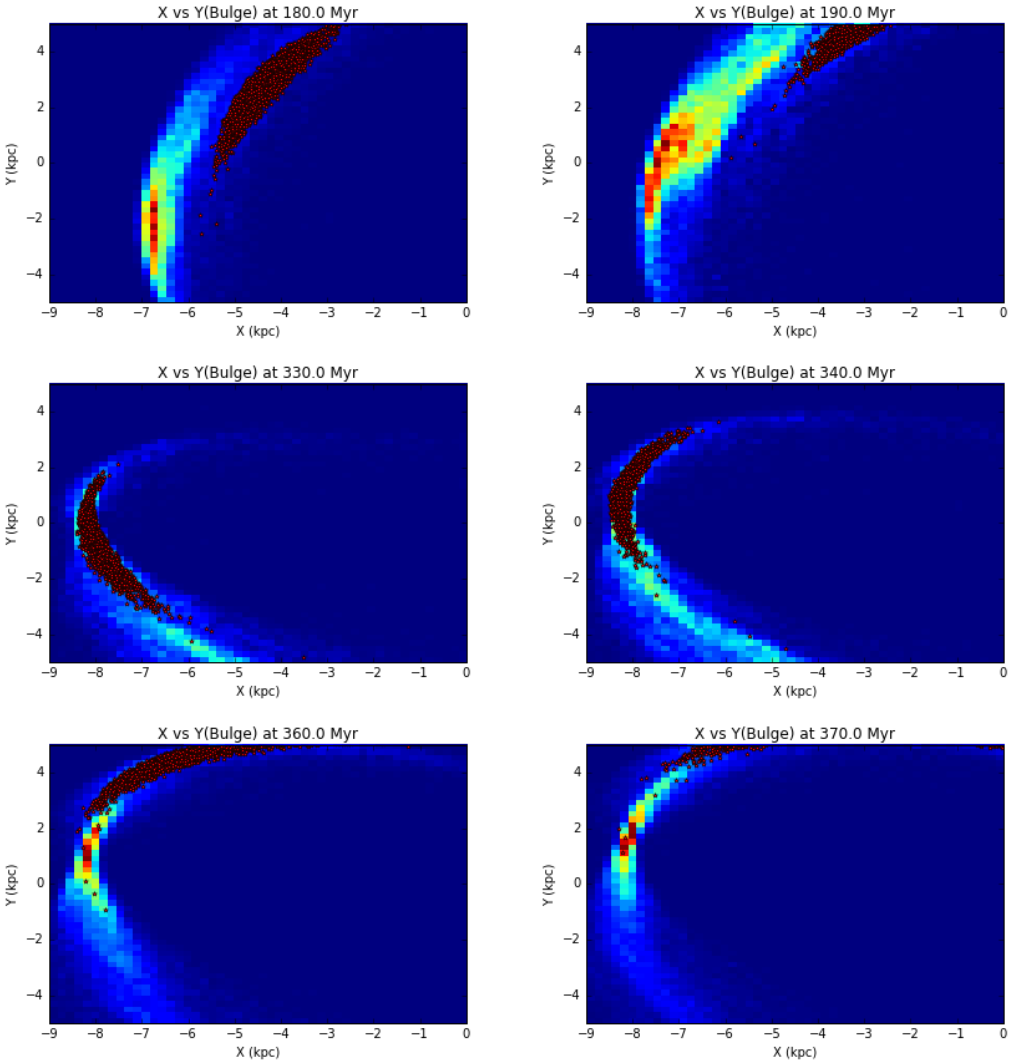

Figure 4.3: Position distributions at different times (Axisymmetric model)

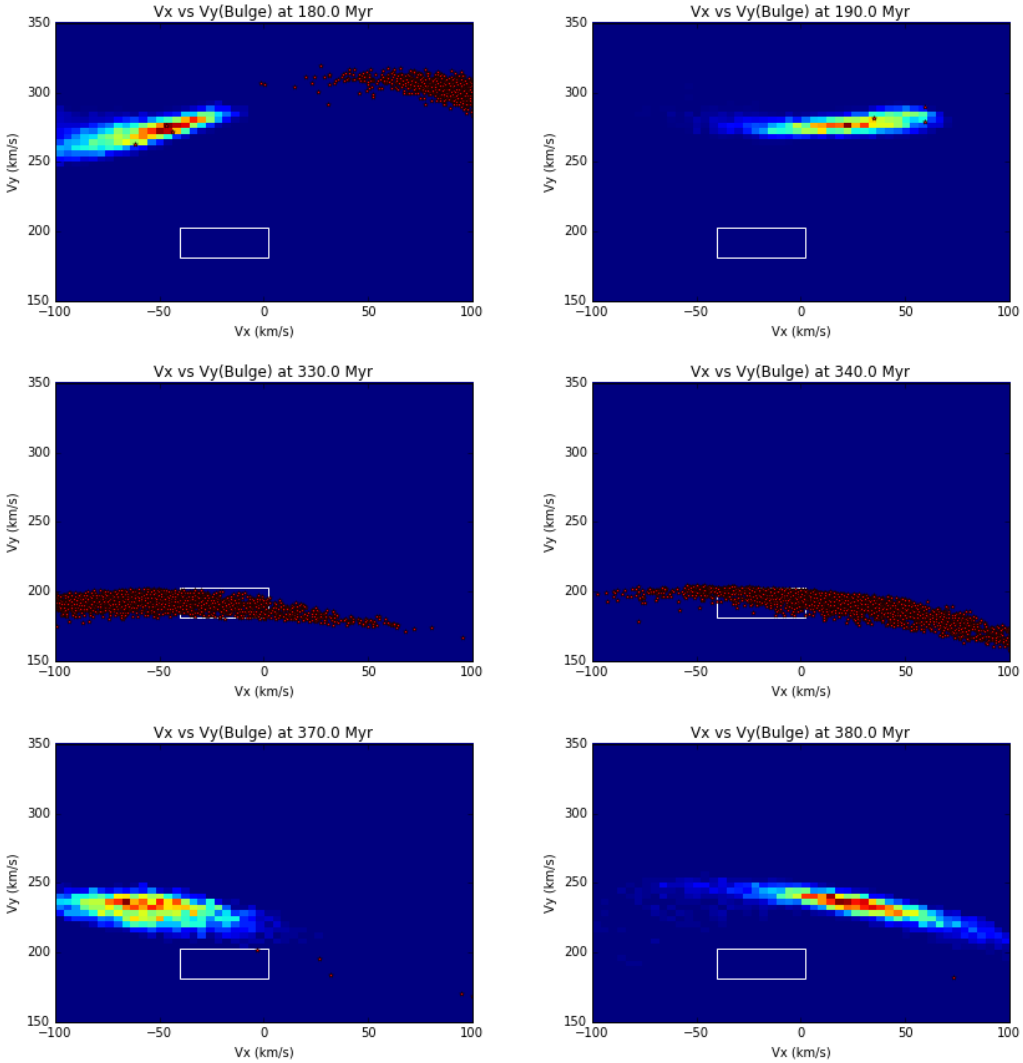

Figure 4.4: Velocity distribution of stars after several azimuthal periods for the stars in the Solar neighbourhood (Axisymmetric model)

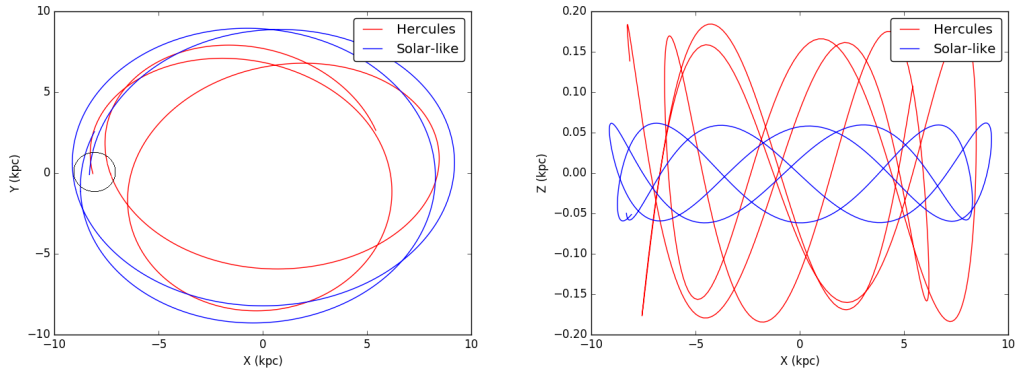

(a) Trajectory in X-Y plane (The circle resembles the SNd)

(b) Trajectory in X-Z plane

Figure 4.5: Trajectories in a long barred potential.

4.2 The Triaxial Bar Potential

I will consider 2 cases here, namely the short bar and the long bar. Since I keep the mass for the bars constant, the short bar will have a higher central density resulting in a different potential.

4.2.1 The Long bar

First I will consider the trajectories. As is visible in Figure 4.5, the Solar-like star is following a close to circular path. This means it almost returns at the same position after several azimuthal periods. Also the oscillations in the z-direction give the image of a very regular orbit. The star from Hercules gives a different picture. The trajectory is far from circular and seems to be more rosette shaped. Compared to the Solar-like star, it also experiences much larger oscillations in the z-direction.

In Figure 4.6 I consider the positions of all the stars in the sample. It is visible that also here the stars in Hercules have a lead on the other stars in the sample. This lead is however less than in the axisymmetric case and the stars from Hercules are still more concentrated.

This also returns in Figure 4.7 where I consider the velocities at the same times. It is clear that the stars in Hercules do still have a bit of an overlap with the stars in the Solar neighbourhood, which is not the case in the axisymmetric model.

It is clearly visible that after 2 azimuthal periods of the stars in Hercules, their velocities are slightly higher than their initial velocities. Some stars do however go through the box, which specifies their initial conditions.

Furthermore it is visible that the velocity distribution after 2 azimuthal periods with respect to the LSR is less smooth than in the axisymmetric case. Where in the axisymmetric case the velocity distribution is a smooth band, in the long barred case it is a more concentrated region in velocity space.

4.2.2 The Short bar

The last case I will discuss is the case in which the central potential is a short bar. The trajectories in Figure 4.8 are very similar to the trajectories of the stars orbiting

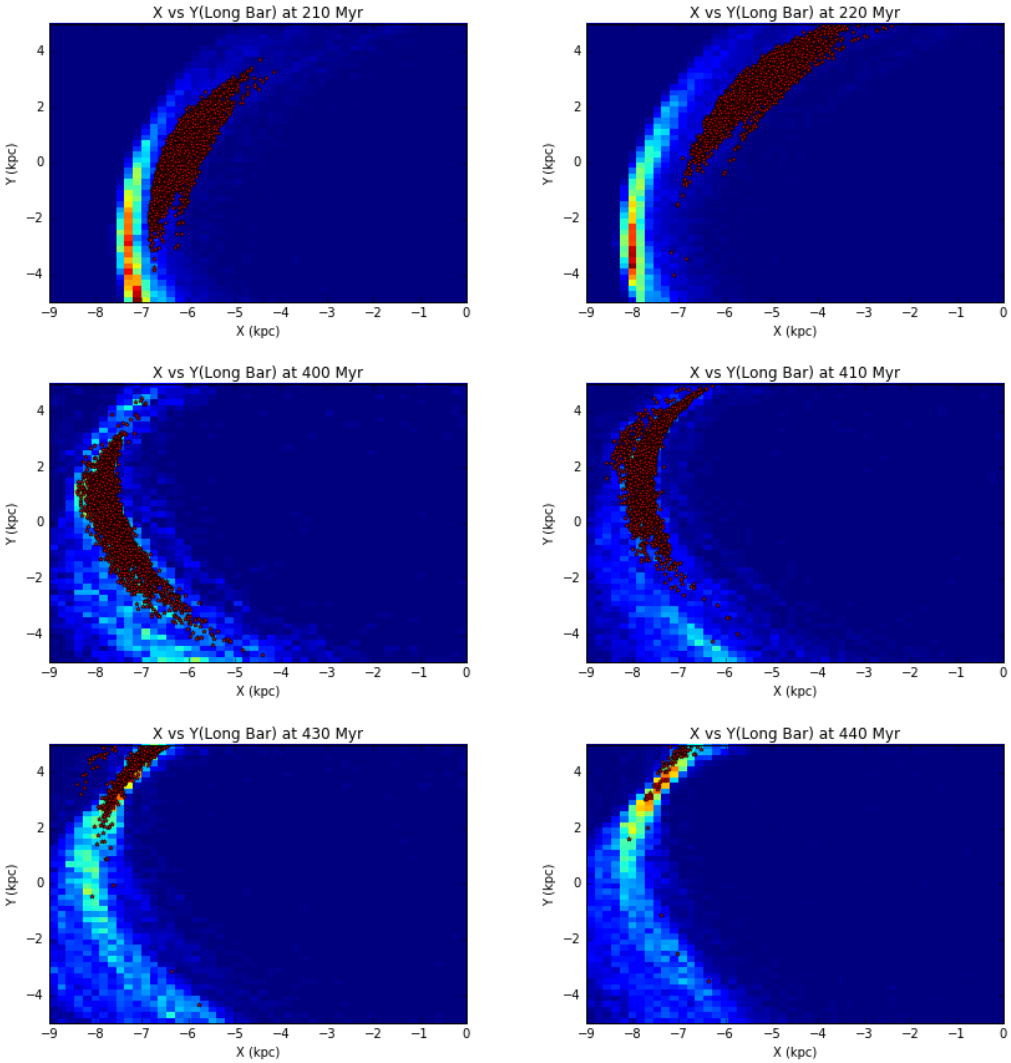

Figure 4.6: Positions for all stars for different times (Long Bar model)

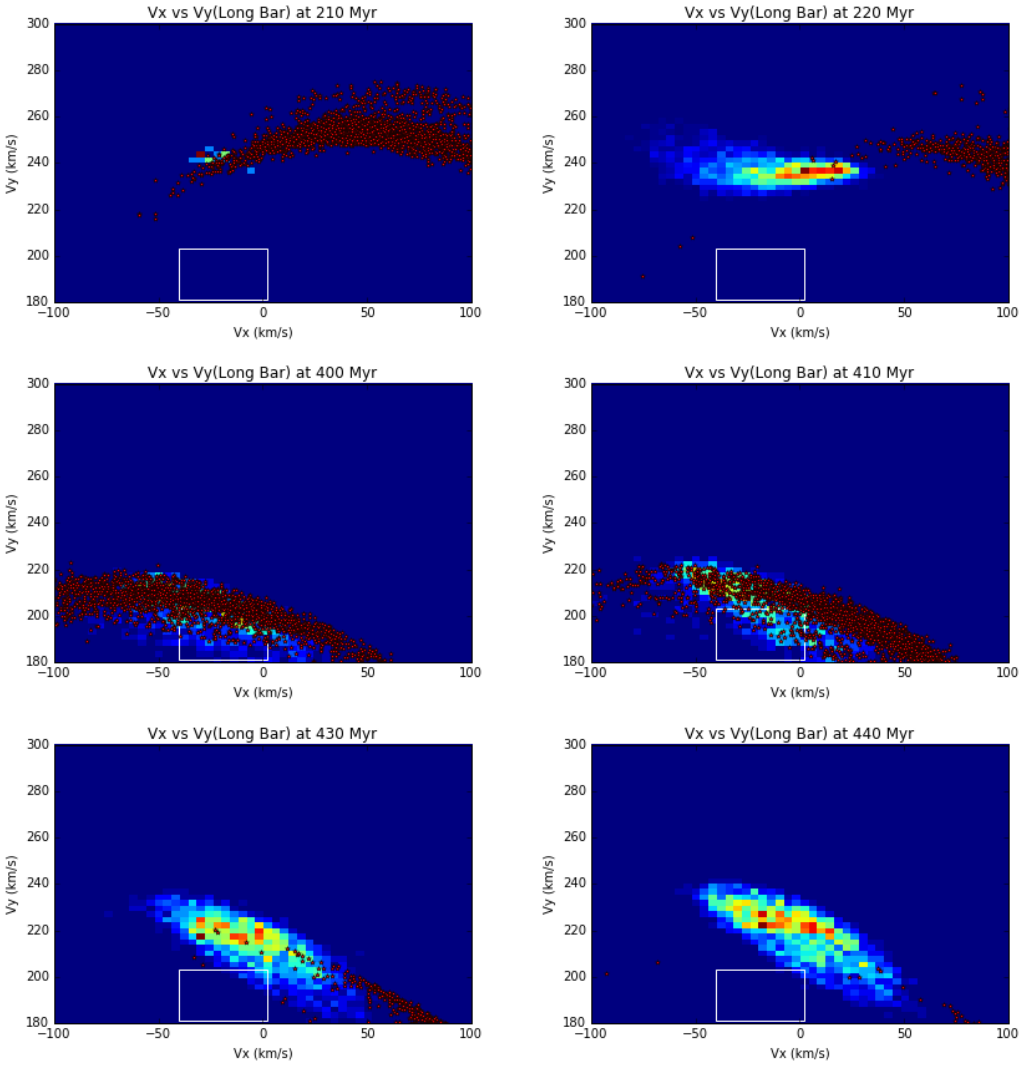

Figure 4.7: Velocity distribution of stars after several azimuthal periods for the stars in the Solar neighbourhood (Long Bar model)

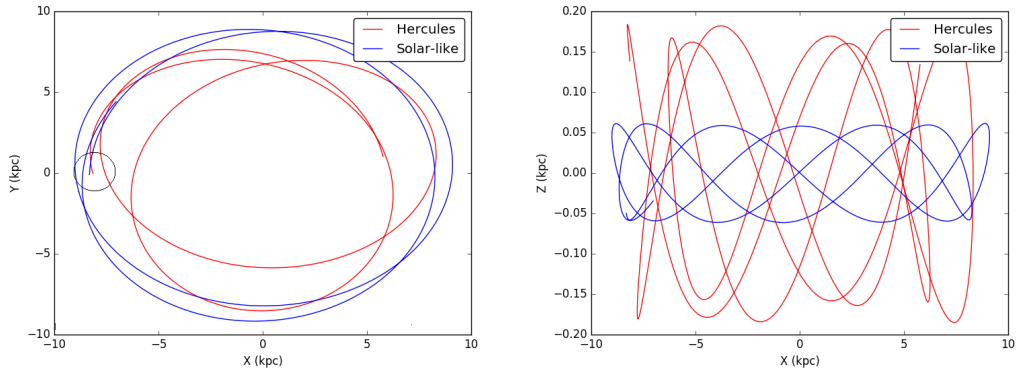

(a) Trajectory in X-Y plane (The circle resembles the SNd)

(b) Trajectory in X-Z plane

Figure 4.8: Trajectories in a short barred potential.

the long bar. The oscillations in the z-direction show only little difference, which is for instance visible in the minima at $x = 3kpc$ and $y = -0.16kpc$.

Now we want to see how the stars behave on the whole in this model. Figure 4.9 shows the distributions of positions for several frames in time.

Once again it is visible that the stars in Hercules have a lead on the LSR. However, the lead in the short barred case is larger than in the long barred case. This can also be seen in the velocity distribution in Figure 4.10 where there is a clear gap between the stars in the Solar neighbourhood and the stars in Hercules.

The cause of this can also be found in Figure 4.5 and 4.8 where the trajectory of the Hercules star in the short barred model is a little bit longer.

From this we can conclude that the stars in the short bar model generally have a shorter azimuthal period than in the long bar model.

Just as in the long barred case, there seems to be a substantial amount of stars from Hercules that do get back in their original velocity range after 2 azimuthal periods with respect to the stars in Hercules. However in the short barred case more stars go through the box than in the long barred case. Comparing the left middle frames in Figures 4.10 and 4.7 this is visible by looking at the boundaries of the box.

A distinction can be made between the barred and axisymmetric cases. In the axisymmetric case stars on circular orbits within the Solar neighbourhood will have similar velocities as the LSR. Their z-angular momentum is conserved in this potential.

However, in the cases of the barred potential, none of the angular momentum components is conserved. This means that objects on a circular orbit in an axisymmetric potential do not correspond to circular orbits in a barred potential. This does of course depend on the mass and the dimensions of the bar, as well as the extent of the orbit.

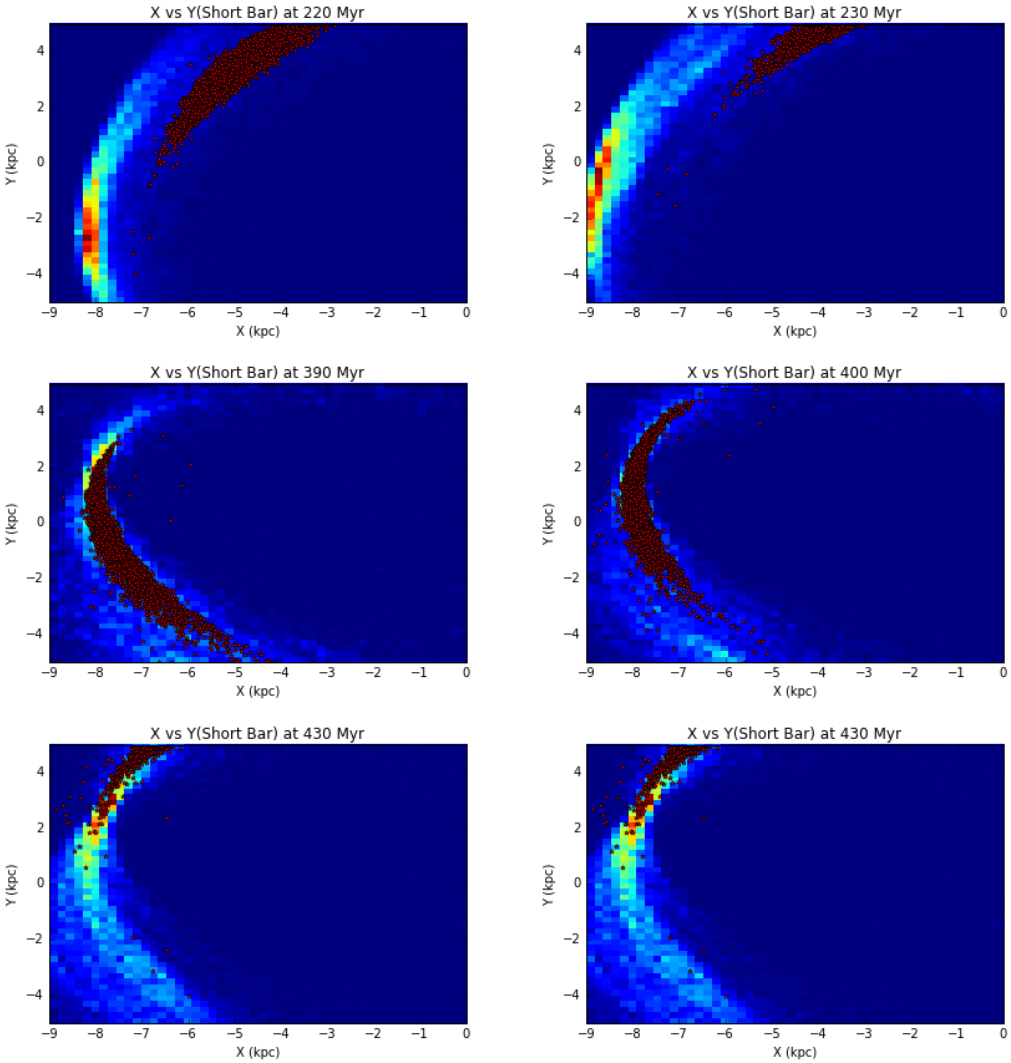

Figure 4.9: Positions for all stars for different times (Short Bar model)

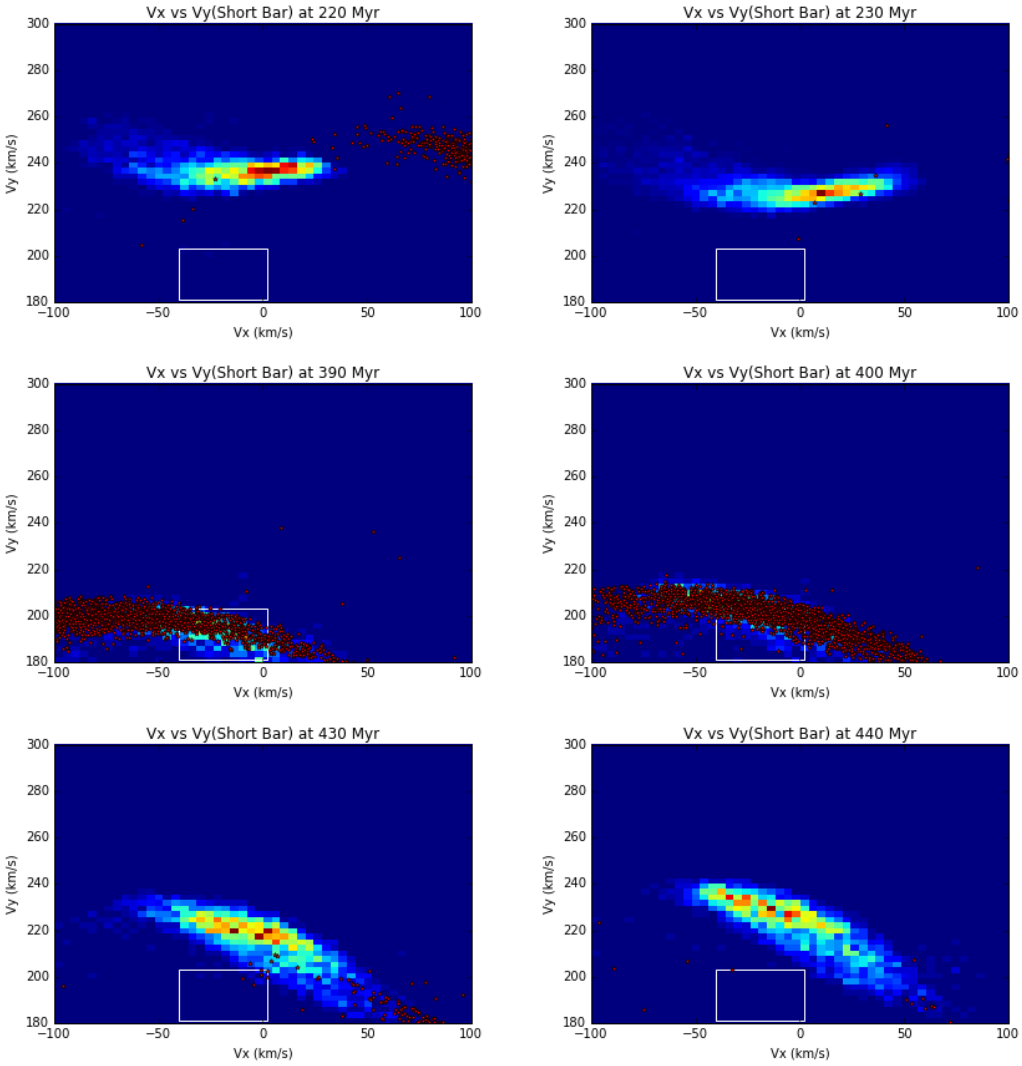

Figure 4.10: Velocity distribution of stars after several azimuthal periods for the stars in the Solar neighbourhood (Short Bar model)

Chapter 5

Conclusion & Discussion

In this research project I have investigated the influence of a long and a short bar on large scale structures in velocity space, such as the Hercules stream and compared that to the results in an axisymmetric potential.

From the results we can draw the following conclusions. The stars in the Hercules stream tend to have a shorter period. Therefore these stars lead the other stars in the sample.

After every even period the stars in Hercules do get back in the same position with the same velocity as they started with. This is visible in the rosette shaped trajectories. Because the z-angular momentum of the stars is too low after 1 azimuthal period, it cannot reach the region that it started in. After 2 azimuthal periods, however, it does have enough z-angular momentum to reach its initial point in space.

For the axisymmetric case the entire stream seems to come back after 2 azimuthal periods. In the cases of the long and the short bar, only part of the stream returns in the same velocity range.

Furthermore it seems that the velocity distributions are smooth rather than that there seems to be structure in it.

An explanation for these results is that Hercules is most probably due to resonances of the bar. Since in this project, I made use of a static bar, there should be no influence from any resonance and hence no substructure.

Another limit in my approach is that the sample of stars I used only contains stars that are within a radius of $300pc$ of the Sun at the present time. This means that I cannot make a full description of the velocity field, since I have too little data.

In order to get a really clear image of the velocity field around the sun, one should do research on a larger sample of stars. In addition, a rotating bar would be more representative in a model for the Milky Way.

Acknowledgements

First of all, I want to express my gratitude to Dr. Lorenzo Posti, for his everlasting patience and helpfulness, throughout the past months. His aid has been of utmost importance for completing this thesis. Second of all, I want to give appreciation to Prof.Dr. Amina Helmi for supporting me and always giving me new insights for improving my work. Her guidelines have kept me on the right way to completing this thesis especially near the end of the project. Also, I want to thank Kevin Bixerman for his willingness to help me with his coding abilities whenever I did not see the right way to fix problems. Lastly I want to thank Reinier Koet and Roland Timmerman for our cooperative behavior the past months revising each others results and shedding new light on small inconveniences.

Appendix A

Code

A.1 Program Explanation

The program we wrote for this research project has a few distinct features that we will carefully explain. It is constructed of multiple scripts, each having their own subject and contribution to the entire project.

The core script is the Leap Frog which imports all the values and calculates the trajectories, generating new data every certain time interval. Thereafter, it will save those values to a file, which we can read out later and analyze the data in it. In this Leap Frog, there is a link to a script containing the total Potential, used to update the velocities. This script imports all the different potentials and adds them through the superposition principle. Consequently, every potential has its own script which is separated from the rest.

Another distinct feature is the separation of constants. Instead of defining every constant in every script, it is more clear to have a separate file containing all the constants, which can be easily called with the '***from** constants **import** **' command. Therefore, changes to the initial values only have to be made once, instead of in every script.

Finally, there is a wide range of scripts analyzing the generated data. This can either be about the conservation laws, but also about the velocity correlations. This is in turn accompanied by a script, which plots the results.

All in all, the big advantage of multiple scripts relative to one large script is clarity. Mistakes can be found more easily by exclusion and adaptations can be made without having to spit through the entire file.

On the next pages you can find the code for the Leap Frog I have written and the scripts for the Ferrers Potential. These two scripts are in my opinion the primary parts of this reseach project. The remaining scripts are mere applications of the generated results and are more generally used.

A.2 Leap Frog

```
from __future__ import print_function, division
import numpy
from constants import *
from FPBar import Force, Potential
from time import clock


def LEAPFROGBAR(x,y,z,vx,vy,vz):
    AA = len(x)
    DATA = numpy.zeros((6, AA))
    EE = numpy.zeros(AA)
    for i in range(len(h)):                          #loop over time
        print(i/2,"Myr")
        if h[i] == 0:                                #set initial conditions
            path = "/net/virgo01/data/users/koot/Data/NonAxi/Short/"
                    +str(i)+"Myr.txt"
            datafile_id = open(path, 'w')
            text = numpy.array(["#", "T", "x","y","z","vx","vy","vz", "E"])
            numpy.savetxt(datafile_id, text, fmt=["%s"],
                          delimiter = ',', newline = '\t')
            empty = numpy.array([0])
            numpy.savetxt(datafile_id, empty, fmt=["%.1e"])
            for j in range(AA):                      #loop over stars
                x1 = x[j]
                y1 = y[j]
                z1 = z[j]
                Fx,Fy,Fz = Force(x1,y1,z1)           #calculate force
                vx1 = vx[j] + k/2*Fx
                vy1 = vy[j] + k/2*Fy
                vz1 = vz[j] + k/2*Fz
                P = Potential(x1,y1,z1)              #calculate potential
                vE = (vx[j]**2+vy[j]**2+vz[j]**2)/2
                E = vE+P

                DATA[0,j] = x1
                DATA[1,j] = y1
                DATA[2,j] = z1
                DATA[3,j] = vx1
                DATA[4,j] = vy1
                DATA[5,j] = vz1
                data = numpy.array([j,h[i],x1,y1,z1,vx1,vy1,vz1])
                numpy.savetxt(datafile_id, data,     #save data to a file
                              delimiter = ',', newline = '\t')
                VCCC = numpy.array([E])
                numpy.savetxt(datafile_id,VCCC)
            datafile_id.close()

        elif h[i] > 0:                               #update each time step
            for j in range(AA):
```

```
            x = DATA[0,j] + k*DATA[3,j]
            y = DATA[1,j] + k*DATA[4,j]
            z = DATA[2,j] + k*DATA[5,j]
            Fx, Fy, Fz = Force(x,y,z)
            vx = DATA[3,j] + k*Fx
            vy = DATA[4,j] + k*Fy
            vz = DATA[5,j] + k*Fz

            DATA[0,j] = x
            DATA[1,j] = y
            DATA[2,j] = z
            DATA[3,j] = vx
            DATA[4,j] = vy
            DATA[5,j] = vz

    if i%2 == 0 and i > 0:                    #save data per 2 timesteps
        path = "/net/virgo01/data/users/koot/Data/NonAxi/Short/"
               +str(i/2)+"Myr.txt"
        datafile_id = open(path, 'w')
        text = numpy.array(["#", "T", "x","y","z","vx","vy","vz", "E"])
        numpy.savetxt(datafile_id, text, fmt=["%s"],
                      delimiter = ',', newline = '\t')
        empty = numpy.array([0])
        numpy.savetxt(datafile_id, empty, fmt=["%.1e"])
        for j in range(AA):
            Fx, Fy, Fz = Force(DATA[0,j],DATA[1,j],DATA[2,j])
            vxE = DATA[3,j] - k/2*Fx
            vyE = DATA[4,j] - k/2*Fy
            vzE = DATA[5,j] - k/2*Fz
            P = Potential(DATA[0,j],DATA[1,j],DATA[2,j])
            vE = (vxE**2+vyE**2+vzE**2)/2
            Enew = vE+P
            if i == 2:
                EE[j] = Enew
            if abs((Enew-EE[j])/Enew) > 0.01:
                print(j,P,vE, Enew, EE[j])
                quit
            data = numpy.array([j,h[i],DATA[0,j],DATA[1,j],DATA[2,j],
                                DATA[3,j],DATA[4,j],DATA[5,j]])
            numpy.savetxt(datafile_id, data,
                          delimiter = ',', newline = '\t')
            VCCC = numpy.array([Enew])
            numpy.savetxt(datafile_id,VCCC)
        datafile_id.close()
return
```

A.3 Ferrers Potential

```
from __future__ import print_function, division

from constants import *
from Wijktest import *
from coef import getcoef

def FPot2(xx,yy,zz):
    x = xx*numpy.cos(phib) - yy*numpy.sin(phib)     #coordinate transformation
    y = xx*numpy.sin(phib) + yy*numpy.cos(phib)
    z = zz
    x2 = x**2
    y2 = y**2
    z2 = z**2

    W100,W001,W000,W010,W011,W101,W110,W200,W020,W002, #get coefficients
    W111,W120,W012,W201,W210,W021,W102,W300,W030,W003 = getcoef(x,y,z)


    P = -C/6*(W000-6*x2*y2*z2*W111+x2*(x2*(3*W200-x2*W300) #calculate potentia
    +3*(y2*(2*W110-y2*W120-x2*W210)-W100))+y2*(y2*(3*W020-y2*W030)
    +3*(z2*(2*W011-z2*W012-y2*W021)-W010))+z2*(z2*(3*W002-z2*W003)
    +3*(x2*(2*W101-x2*W201-z2*W102)-W001)))
    return P

def FF2(xx,yy,zz):
    x = xx*numpy.cos(phib) - yy*numpy.sin(phib)     #coordinate transformation
    y = xx*numpy.sin(phib) + yy*numpy.cos(phib)
    z = zz
    x2 = x**2
    y2 = y**2
    z2 = z**2

    W100,W001,W000,W010,W011,W101,W110,W200,W020,W002, #get coefficients
    W111,W120,W012,W201,W210,W021,W102,W300,W030,W003 = getcoef(x,y,z)

    Fxx = -x*C*(W100+x2*(x2*W300+2*(y2*W210-W200))  #calculate forces
          +y2*(y2*W120+2*(z2*W111-W110))
          +z2*(z2*W102+2*(x2*W201-W101)))
    Fyy = -y*C*(W010+x2*(x2*W210+2*(y2*W120-W110))
          +y2*(y2*W030+2*(z2*W021-W020))
          +z2*(z2*W012+2*(x2*W111-W011)))
    Fzz = -z*C*(W001+x2*(x2*W201+2*(y2*W111-W101))
          +y2*(y2*W021+2*(z2*W012-W011))
          +z2*(z2*W003+2*(x2*W102-W002)))

    Fx = Fxx*numpy.cos(-phib) - Fyy*numpy.sin(-phib) #back transformation
    Fy = Fxx*numpy.sin(-phib) + Fyy*numpy.cos(-phib)

    return Fx,Fy,Fzz
```

A.4 Ferrers addition I

```
from __future__ import print_function, division
import scipy as sp
from scipy import optimize as o
import numpy as np
from constants import *


def lfunc(u,x,y,z):                                    #function m(lambda)
    return (x**2/(Fa**2+u)+y**2/(Fb**2+u)+z**2/(Fc**2+u))-1

def lamb(x,y,z):                                       #find lambda
    lfind = o.fsolve(lambda u: lfunc(u,x,y,z), 0)
    return lfind

def wijk(u,i,j,k):                                     #coefficient formula
    if (Fa2+u)*(Fb2+u)*(Fc2+u)<0:
        print(i,j,k)

    return (Fa2+u)**(-i)*(Fb2+u)**(-j)*(Fc2+u)**(-k)
           *((Fa2+u)*(Fb2+u)*(Fc2+u))**(-0.5)

def W(lamb, i,j,k):                                    #calculate coefficient
    return sp.integrate.quad(wijk, lamb, np.inf, args=(i,j,k))[0]

def dlam(L):                                           #denominator integral
    return np.sqrt((Fa2+L)*(Fb2+L)*(Fc2+L))
```

A.5 Ferrers addition II

```
from __future__ import print_function, division
import numpy
from Wijktest import dlam, lamb, W
from constants import *

def getcoef(x,y,z):                                    #calculating coefficient
    lam = lamb(x,y,z)                                  #define lambda

    if abs(x) <= Fa and abs(y) <= Fb and abs(z) <= Fc:
        lam = 0
    W100, W001, W000 = W(lam,1,0,0), W(lam,0,0,1), W(lam,0,0,0)
    W010 = (2/dlam(lam))-W100-W001                     #recurrent relations
    W011 = (W001-W010)/(Fb**2-Fc**2)
    W101 = (W100-W001)/(Fc**2-Fa**2)
    W110 = (W010-W100)/(Fa**2-Fb**2)

    LA = lam+Fa2
    LB = lam+Fb2
    LC = lam+Fc2


    W200 = ((2/(dlam(lam)*LA))-W110-W101)/3
    W020 = ((2/(dlam(lam)*LB))-W011-W110)/3
    W002 = ((2/(dlam(lam)*LC))-W101-W011)/3

    W111 = (W110-W011)/(Fc**2-Fa**2)
    W120 = (W020-W110)/(Fa**2-Fb**2)
    W012 = (W002-W011)/(Fb**2-Fc**2)
    W201 = (W200-W101)/(Fc**2-Fa**2)
    W210 = (W110-W200)/(Fa**2-Fb**2)
    W021 = (W011-W020)/(Fb**2-Fc**2)
    W102 = (W101-W002)/(Fc**2-Fa**2)
    W300 = ((2/(dlam(lam)*LA**2))-W210-W201)/5
    W030 = ((2/(dlam(lam)*LB**2))-W021-W120)/5
    W003 = ((2/(dlam(lam)*LC**2))-W102-W012)/5


    return W100,W001,W000,W010,W011,W101,W110,W200,W020,W002,W111,W120,W012,
           W201,W210,W021,W102,W300,W030,W003
```

Bibliography

Antoja, T. et al. (2014). "Constraints on the Galactic bar from the Hercules stream as traced with RAVE across the Galaxy". In: *Astronomy & Astrophysics* 563, A60.

Becker, W. and G. Contopoulos (2012). *The Spiral Structure of Our Galaxy*. Vol. 38. Springer Science & Business Media.

Bensby, T. et al. (2007). "Disentangling the Hercules stream". In: *The Astrophysical Journal Letters* 655.2, p. L89.

Binney, J., O. Gerhard, and D. Spergel (1997). "The photometric structure of the inner Galaxy". In: *Monthly Notices of the Royal Astronomical Society* 288.2, pp. 365–374.

Binney, J. and S. Tremaine (2011). *Galactic dynamics*. Princeton university press.

Bissantz, N. and O. Gerhard (2002). "Spiral arms, bar shape and bulge microlensing in the Milky Way". In: *Monthly Notices of the Royal Astronomical Society* 330.3, pp. 591–608.

Blitz, L. and D. N. Spergel (1991). "Direct evidence for a bar at the Galactic center". In: *The Astrophysical Journal* 379, pp. 631–638.

Bovy, J. (2010). "Tracing the Hercules stream around the galaxy". In: *The Astrophysical Journal* 725.2, p. 1676.

Cohen, R. and R. Few (1976). "Observations of OH in the Galactic Centre". In: *Monthly Notices of the Royal Astronomical Society* 176.3, pp. 495–523.

De Vaucouleurs, G (1964). "Interpretation of velocity distribution of the inner regions of the Galaxy". In: *Symposium-International Astronomical Union*. Vol. 20. Cambridge Univ Press, pp. 195–199.

Dehnen, W. (2000). "The effect of the outer Lindblad resonance of the galactic bar on the local stellar velocity distribution". In: *The Astronomical Journal* 119.2, p. 800.

Eggen, O. J. (1958). "Stellar groups. II. The ζ Herculis, ϵ Indi and 61 Cygni Groups of High-Velocity Stars". In: *Monthly Notices of the Royal Astronomical Society* 118.2, pp. 154–160.

ESA (2005). *Gaia mission*. URL: http://www.esa.int/Our_Activities/Space_Science/Exploring_space/Mapping_the_Galaxy_and_watching_our_backyard (visited on 06/25/2005).

Famaey, B., A. Siebert, and A. Jorissen (2008). "On the age heterogeneity of the Pleiades, Hyades, and Sirius moving groups". In: *Astronomy & astrophysics* 483.2, pp. 453–459.

Famaey, B. et al. (2005). "Local kinematics of K and M giants from CORAVEL/Hipparcos/Tycho-2 data-Revisiting the concept of superclusters". In: *Astronomy & astrophysics* 430.1, pp. 165–186.

Hernquist, L. (1990). "An analytical model for spherical galaxies and bulges". In: *The Astrophysical Journal* 356, pp. 359–364.

Krumholtz, M. (2015). *Leap Frog Method image*. URL: https://sites.google.com/a/ucsc.edu/krumholz/teaching-and-courses/ast119_w15/class-11 (visited on 06/01/2017).

Kuzmin, G. (1956). "Model of the steady galaxy allowing of the triaxial distribution of velocities". In: *Astronomicheskii Zhurnal* 33, p. 27.

Landau, L. (1969). *Mechanics*. Pergamon Press.

Liszt, H. and W. Burton (1980). "The gas distribution in the central region of the Galaxy. III-A barlike model of the inner-Galaxy gas based on improved HI data". In: *The Astrophysical Journal* 236, pp. 779–797.

Michalik, D., L. Lindegren, and D. Hobbs (2015). "The Tycho-Gaia astrometric solution-How to get 2.5 million parallaxes with less than one year of Gaia data". In: *Astronomy & Astrophysics* 574, A115.

Miyamoto, M. and R. Nagai (1975). "Three-dimensional models for the distribution of mass in galaxies". In: *Publications of the Astronomical Society of Japan* 27, pp. 533–543.

Monari, G. et al. (2017). "Tracing the Hercules stream with Gaia and LAMOST: new evidence for a fast bar in the Milky Way". In: *Monthly Notices of the Royal Astronomical Society: Letters* 466.1, pp. L113–L117.

Navarro, J. F. (1996). "The structure of cold dark matter halos". In: *Symposium-international astronomical union*. Vol. 171. Cambridge Univ Press, pp. 255–258.

Pearson (2008). *Pearson Education*. Pearson Addison-Wesley.

Pérez-Villegas, A. et al. (2017). "Revisiting the Tale of Hercules: how stars orbiting the Lagrange points visit the Sun". In: *The Astrophysical Journal Letters* 840.1, p. L2.

Peters III, W. L. (1975). "Models for the inner regions of the Galaxy. I". In: *The Astrophysical Journal* 195, pp. 617–629.

Pfenniger, D (1984). "The 3D dynamics of barred galaxies". In: *Astronomy and Astrophysics* 134, pp. 373–386.

Plummer, H. C. (1911). "On the problem of distribution in globular star clusters". In: *Monthly notices of the royal astronomical society* 71, pp. 460–470.

Raboud, D. et al. (1998). "Evidence for a signature of the galactic bar in the solar neighbourhood". In: *arXiv preprint astro-ph/9802266*.

RAVE (2014). *RAVE-the Radial Velocity Experiment*. URL: https://www.rave-survey.org/project/ (visited on 2014).

Schönrich, R. (2012). "Galactic rotation and solar motion from stellar kinematics". In: *Monthly Notices of the Royal Astronomical Society* 427.1, pp. 274–287.